Statistically Relevant Conserved Quantities for Truncated Quasi-Geostrophic Flow

Rafail V. Abramov and Andrew J. Majda[1]

Courant Institute of Mathematical Sciences and Center for Atmosphere and Ocean Sciences, New York University, New York, NY 10012

Contributed by Andrew J. Majda, January 24, 2003

Systematic applications of ideas from equilibrium statistical mechanics lead to novel promising strategies for assessing the unresolved scales of motion in many problems in science and engineering. A scientific debate over more than the last twenty-five years involves which conserved quantities among the formally infinite list are statistically relevant for the large scale equilibrium statistical behavior. Here this important issue is addressed by utilizing suitable discrete numerical approximations for geophysical flows with many conserved quantities as a numerical laboratory. The results of numerical experiments are presented here for these truncated geophysical flows with topography in a suitable regime. These experiments establish that the integrated third power of potential vorticity besides the familiar constraints of energy, circulation, and enstrophy (the integrated second power) is statistically relevant in this regime for the coarse-grained equilibrium statistical behavior at large scales. Furthermore, the integrated higher powers of potential vorticity larger than three are statistically irrelevant for the large scale equilibrium statistical behavior in the examples studied here.

Geophysical flows provide an important prototype context for developing new methods for underresolved models in science and engineering. The wide range of unresolved scales of motion with highly inhomogeneous behavior for the atmosphere and ocean on earth as well as for other planets like Jupiter, require novel statistical strategies to assess the nontrivial impact of these unresolved features on the larger scales. Novel systematic applications of ideas from equilibrium statistical mechanics to these inhomogeneous geophysical flows have lead to promising new statistical strategies for the ocean (1–4), the atmosphere (5, 6), and the giant planets such as Jupiter (7) in agreement with contemporary observations. These different equilibrium statistical theories all attempt to predict the coarse-grained behavior at large scales through use of some of the formally infinite list of conserved quantities for idealized geophysical flow; this has been a topic of continuous debate over more than the last twenty-five years in the fluid dynamics community (8–14) and represents the main topic of the present work. Here the results of numerical experiments are presented for truncated geophysical flows with topography in a suitable regime which establish that the integrated third power of potential vorticity besides the familiar constraints of energy, circulation, and enstrophy is statistically relevant for the coarse-grained equilibrium statistical behavior at large scales. Furthermore, in this regime of fluid motion the integrated higher powers of potential vorticity larger than three are statistically irrelevant for the large scale equilibrium statistical behavior. This is the first unambiguous numerical evidence of the nontrivial role of the higher invariants for inviscid truncated geophysical flows for coarse-grained large scale equilibrium statistical behavior. The simplest geophysical model utilized here is barotropic two-dimensional flow with topography in periodic geometry, which is described by the equations

$$\begin{aligned} q &= \Delta\psi + h, \\ \vec{v} &= \nabla^{\perp}\psi = \begin{pmatrix} -\psi_y \\ \psi_x \end{pmatrix}, \\ \frac{\partial q}{\partial t} &+ \vec{v}\,\nabla q = 0. \end{aligned} \qquad \textbf{[1]}$$

In **1**, q is the potential vorticity, $\omega = \Delta\psi$ is the relative vorticity, $\vec{v}$ is the incompressible fluid velocity, ψ is the stream function, and h is the prescribed topography. When h is zero, **1** become the equations for 2D incompressible flow. Non-zero topography often has profound impact on the large scale flow (11–14). Here and below we assume a 2π-periodic geometry in both the x and y variables which are also denoted by x_1, x_2 whenever convenient. The equations in **1** conserve kinetic energy,

$$\begin{aligned} E = \frac{1}{2}\int_{T^2}|\vec{v}|^2 &= -\frac{1}{2}\int_{T^2}\psi\omega = \\ &= -\frac{1}{2}\int_{T^2}\psi(q-h), \end{aligned} \qquad \textbf{[2]}$$

as well as the infinite number of conserved quantities,

$$Q_p(q) = \int_{T^2} q^p, \quad p = 1, 2, 3, \ldots. \qquad \textbf{[3]}$$

In **2**, **3**, $\int_{T^2}\cdot$ denotes integration over the period domain in periodic geometry, where the total circulation, Q_1, satisfies $Q_1 \equiv 0$. The quadratic conserved quantity, the enstrophy

$$\mathcal{E} = \frac{1}{2}Q_2(q), \qquad \textbf{[4]}$$

is singled out in some statistical theories for large scale flow (8,10–12,14,15) as having special significance, while the higher generalized enstrophies, $Q_p(q)$, for $p \geq 3$ are ignored in these theories. Other researchers (16) claim that the entire infinite list of conserved quantities in **3** is statistically significant for describing the coarse-grained features at large scales. A third group (17, 18) invokes the central role of point vortex dynamics with three conserved quantities in large scale statistical behavior, but with $Q_p(q)$ formally infinite for $p \geq 2$. Finally, a fourth statistical approach has evolved recently (2, 3, 7, 19), where the energy and circulation are imposed on the large scale flow while a suitable prior distribution is utilized to encode the potential vorticity fluctuations at small scales. These various statistical theories, their relative strength and weakness, new statistical approaches and potential applications are discussed by Majda and Wang (13) in a recent monograph which contains many additional references and discussion. One way to address these issues is to study the statistical behavior of discrete approximations to **1** conserving the energy in **2**, and in addition other discrete approximations to the generalized enstrophies in **3**. This is the main topic in subsequent sections of this paper.

[1]To whom reprints should be addressed. E-mail: jonjon@cims.nyu.edu

The Traditional Spectral Truncation and Equilibrium Statistical Theory

The potential vorticity, q, in **1** is truncated by projection onto $(2M+1)\times(2M+1)$ Fourier modes by the projection operator

$$P_\varepsilon q = \sum_{|k_1|,|k_2|\le M} \hat{q}_{\mathbf{k}} e^{i\vec{x}\mathbf{k}}, \quad \varepsilon = \frac{2\pi}{2M+1}. \qquad \textbf{[5]}$$

The traditional aliased truncation of the quasi-geostrophic equations in **1** for these Fourier coefficients $\hat{q}_{\mathbf{k}}$, $|k_1| \le M$, $|k_2| \le M$, is given by

$$\frac{\mathrm{d}\hat{q}_{\mathbf{k}}}{\mathrm{d}t} = \sum_{|k_1'|,|k_2'|\le M} \frac{\mathbf{k}\times\mathbf{k}'}{|\mathbf{k}'|^2}\hat{q}_{\mathbf{k}+\mathbf{k}'}(\hat{q}_{-\mathbf{k}'} - \hat{h}_{-\mathbf{k}'}). \qquad \textbf{[6]}$$

In **6** the finite domain of the Fourier coefficients is extended to $(4M+1)\times(4M+1)$ by using the periodicity rule $\hat{q}_{\mathbf{k}} = \hat{q}_{\mathbf{k}+2M+1}$. It is well-known (10, 12, 13, 20) that the traditional spectral truncation in **6** conserves energy, circulation, and enstrophy from **2**-**4** but in general none of the higher order invariants in **3** for $p \ge 3$; this last fact has been demonstrated in recent numerical experiments (20,21). The energy-enstrophy statistical theory which utilizes only these two conserved quantities for the truncation in **6** predicts a Gaussian probability measure for the equilibrium statistical behavior of the Fourier modes (10–13). Recall that Gaussian measures are uniquely characterized by their mean and variance. Given externally prescribed mean values for the energy and enstrophy, the mean of this probability distribution for $\hat{q}_{\mathbf{k}}$ is determined by the linear equation,

$$\bar{q}_\mu = \Delta\bar{\psi}_\mu + h = \mu\bar{\psi}_\mu, \qquad \textbf{[7]}$$

while there is equipartition of pseudo-energy of perturbations around the mean state in **7** with a constant variance $\alpha > 0$. Here the pseudo-energy Fourier coefficients, $\hat{p}_{\mathbf{k}}$, are given by

$$\hat{p}_{\mathbf{k}} = \left(1 + \frac{\mu}{|\mathbf{k}|^2}\right)^{1/2}\hat{\omega}_{\mathbf{k}}, \qquad \textbf{[8]}$$

with $\hat{\omega}_{\mathbf{k}}$ being the Fourier coefficients of relative vorticity. The constants, μ and α, completely characterizing the Gaussian measure, are determined by the values of E and $\mathcal{E}$. A wide variety of numerical experiments with the truncation in **6** (12, 13, 15) confirm the predictions of the equilibrium statistical theory from **7** and **8**. However, these results cannot address the fundamental issue for the statistical relevance of the higher order invariants in **3** for $p \ge 3$ since these fail to be conserved by the approximation in **6** over long time intervals of integration. Here, the equilibrium statistical predictions through **7** and **8** are regarded as a null hypothesis in the tests reported below for the role of the higher order invariants.

The Spectral Truncation with Many Conserved Quantities

Here, following the important observation by Zeitlin (22), we consider the sine-bracket truncation as an approximation to the quasi-geostrophic dynamics in **1** through the spectral approximation in **6**. This finite dimensional set of equations for the Fourier coefficients is given by

$$\frac{\mathrm{d}\hat{q}_{\mathbf{k}}}{\mathrm{d}t} = \sum_{k_1',k_2'=-M}^{M} \frac{\sin(\varepsilon\mathbf{k}\times\mathbf{k}')}{\varepsilon|\mathbf{k}'|^2}\hat{q}_{\mathbf{k}+\mathbf{k}'}(\hat{q}_{-\mathbf{k}'} - \hat{h}_{-\mathbf{k}'}), \qquad \textbf{[9]}$$
$$\varepsilon = \frac{2\pi}{2M+1},$$

with the same convention of periodicity as in **6**. The truncation in **9** conserves the energy in **2** as the Hamiltonian. In addition, the sine-bracket truncation in **9** conserves $2M$ invariants of the form

$$C_N = \sum_{Z^N} \hat{q}_{\mathbf{i}_1}\ldots\hat{q}_{\mathbf{i}_N}\cos[\varepsilon A(\mathbf{i}_1,\ldots,\mathbf{i}_N)],$$
$$Z^N = \{(\mathbf{i}_1,\ldots,\mathbf{i}_N), \sum_{j=1}^{N}\mathbf{i}_j = \mathbf{0}\}, \qquad \textbf{[10]}$$
$$1 \le N \le 2M,$$
$$A(\mathbf{i}_1,\ldots,\mathbf{i}_N) = \mathbf{i}_2\times\mathbf{i}_1 + \mathbf{i}_3\times(\mathbf{i}_1+\mathbf{i}_2) + \ldots + \mathbf{i}_N\times(\mathbf{i}_1+\ldots+\mathbf{i}_{N-1}).$$

The Casimir invariant C_2 is a multiple of the enstrophy since $A(\mathbf{i},-\mathbf{i}) = 0$. However, the higher Casimir invariants C_N for $3 \le N \le 2M$ are suitable regularizations of those in **3** for $3 \le p \le 2M$. A pedagogical detailed discussion of **9**, **10**, as well as related numerical issues used below can be found in (13, 20, 21). In particular, to guarantee conservation of the invariants in **10** within roundoff error under time discretization, McLachlan's (23) symplectic integrator is combined with a suitable version of second order accurate Strang splitting in time (20, 21). This last modification of the basic algorithm in (23) is crucial for accurate energy conservation and results in a 10^{-4} decrease in relative errors for the energy with the time steps used below for only twice the computational expense.

Numerical Experiments Demonstrating the Statistical Relevance of $C_3(q)$ at Large Scales

In the numerical experiments reported here, the prescribed values of the initial data were chosen so that the energy and enstrophy were fixed at $E = 7$ and $\mathcal{E} = 20$ while the value of the third invariant, $C_3(q)$ from **10**, normalized through $\hat{C}_3(q) = C_3(q)/\mathcal{E}^{3/2}$, varied through the four values, $\hat{C}_3 = 0,\ 2,\ 4,\ 6$. A standard constrained optimization problem was set up to find initial data with many Fourier modes satisfying these constraints (21). The higher order invariants, C_N, for $4 \le N \le 2M$ were not specified by pre-determined values for the initial data although they are automatically conserved within roundoff error for the algorithm in **9**. The values of energy and enstrophy, $E = 7$, $\mathcal{E} = 20$, guarantee a suitable "negative temperature regime" (11–13) for the energy-enstrophy equilibrium statistical theory summarized in **7**, **8** with $\mu \cong -0.9$, $\alpha \cong 20$. The numerical experiments utilizing **9** reported below use $M = 11$ so that there are 528 active Fourier modes and 22 nontrivial conserved quantities in the dynamics. In all numerical experiments reported below, the equations in **9** were calculated for times of order 10^4 with a time step, $\Delta t = 0.01$ with a maximum relative error in energy of $1.2\cdot 10^{-6}$. Statistics were gathered through long-time averaging of individual solutions with

$$\langle f\rangle_\tau = \frac{1}{\tau}\int_{T_0}^{T_0+T} f(t)\,\mathrm{d}t \qquad \textbf{[11]}$$

denoting the averaging window. After several initial experiments, it was determined that initial times T_0 with $T_0 \ge 10^3$ were sufficiently long to begin the time-averaging procedure. Three different cases of barotropic geophysical flow from **1** with the discretization from **9** were studied with the above parameters for the initial data: no topography, large scale random topography with non-zero Fourier modes at $|\mathbf{k}|^2 = 2, 4$, and the deterministic layered topography, $h = 0.2\cos(x) + 0.4\cos(2x)$. This last case has the advantage in display that the energy-enstrophy

theory in **7**, **8** predicts a large scale mean flow which is also layered, so $\bar{\psi}(x)$ is a function of the x-variable alone, for any value of μ; thus, significant departures from such a layered structure in x in stream function plots provide strong visual evidence for departures in the large-scale statistical predictions beyond the energy-enstrophy theory. Most of the results are reported below for this case to take advantage of this fact. Since the focus here is on the statistical relevance of the higher order invariants in **3** or **10** for equilibrium statistical theories, a higher order invariant is called statistically relevant at large scales if it affects single-point spatial statistics such as the large scale mean, energy spectrum, and probability distribution function (PDF) centered about the mean. For example, the effect of the higher order invariants for **9** on two-point spatial correlations is ignored here. With all of this background, next results are reported below for the mixing properties of the system, the energy spectrum, the mean stream function, the mean potential vorticity, and the PDF for potential vorticity.

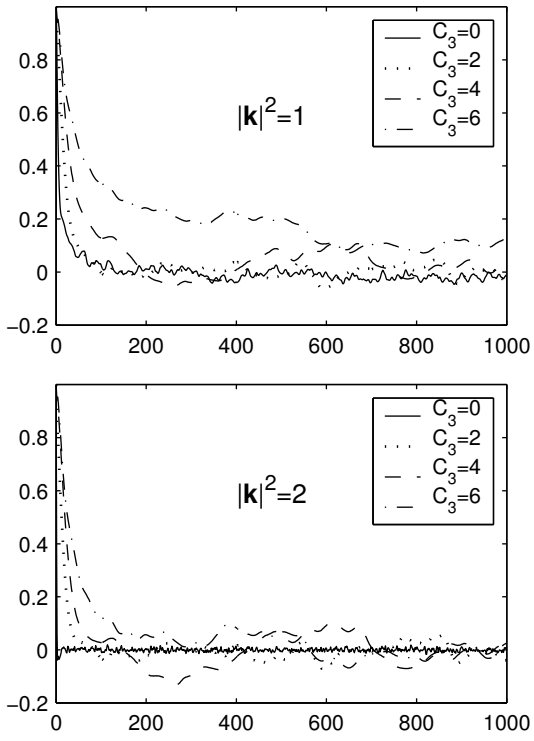

Fig. 1. Averaged temporal correlations for $|\mathbf{k}|^2 = 1$ and $|\mathbf{k}|^2 = 2$ for varying values of skewness, $\hat{C}_3 = 0,\ 2,\ 4,\ 6$.

Mixing and Decay of Temporal Correlations

The normalized temporal correlation functions averaged over the two groups of Fourier modes $|\mathbf{k}|^2 = 1$ and $|\mathbf{k}|^2 = 2$ are depicted in Fig. 1 for the four cases with varying $\hat{C}_3$ for layered topography. These are the correlation functions with the slowest decay rate among all the groups of 528 Fourier modes with significantly faster decay for time correlations of the higher modes not depicted here. Obviously, the longest tails for the correlations occur for $|\mathbf{k}|^2 = 1$. The two graphs in Fig. 1 each have four curves with the cases $\hat{C}_3 = 0$ demonstrating the most rapid decay of correlations, $\hat{C}_3 = 2, 4$ exhibiting clear decay of correlations, and the case $\hat{C}_3 = 6$ with $|\mathbf{k}|^2 = 1$ showing marginal decay of correlations to below 15% of the value with zero lag at time lags of 10^3. The correlation function in this case eventually decays to zero with time lags of order $2 \cdot 10^3$ but the similar plot for $|\mathbf{k}|^2 = 1$ with $\hat{C}_3 = 8$, not depicted here, exhibits no decay of correlations. Thus the value $\hat{C}_3 = 6$ is near the boundary of the parameter regime with decay of temporal correlations. The decay of correlations of Fourier modes is the most primitive test for mixing in phase space of an individual solution (13, 24–26) and justifies the use of the time averages in **11** in calculating statistics of the mean flow and energy spectrum. The other cases with no topography and random topography have similar behavior in the decay of temporal correlations (21).

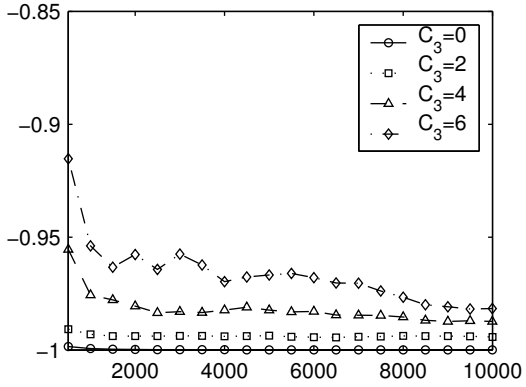

Fig. 2. The graphical correlation, $C(\langle\psi\rangle_\tau, \langle q\rangle_\tau)$, as a function of the averaging window, τ, $\hat{C}_3 = 0,\ 2,\ 4,\ 6$.

The Large Scale Mean Flow

Here the large scale mean flow is calculated from the numerical solution by processing the time average of the stream function, $\bar{\psi} = \langle\psi\rangle_\tau$ and $\bar{q} = \langle q\rangle_\tau$ at individual spatial points and comparing the results. If the energy and enstrophy are the only important conserved quantities, then the energy-enstrophy statistical theory in **7** predicts that $\langle\psi\rangle_\tau$ and $\langle q\rangle_\tau$ should become increasingly collinear as τ increases. This is quantified by measuring the graphical correlation between $\langle\psi\rangle_\tau$ and $\langle q\rangle_\tau$, defined by

$$C(\langle\psi\rangle_\tau, \langle q\rangle_\tau) = \frac{(\langle\psi\rangle_\tau, \langle q\rangle_\tau)_0}{\|\langle\psi\rangle_\tau\|\|\langle q\rangle_\tau\|} \qquad \textbf{[12]}$$

with $(f,g)_0 = \int_{T^2} fg$, $\|f\| = (f,f)_0^{1/2}$. Note that solutions of the energy-enstrophy statistical theory in **7** with $\mu < 0$ are collinear and satisfy $C(\bar{\psi}_\mu, \bar{q}_m u) = -1$. In Fig. 2, the behavior of the graphical correlation $C(\langle\psi\rangle_\tau, \langle q\rangle_\tau)$ is depicted as a function of the averaging window, τ, in **11** for $10^3 \le \tau \le 10^4$ for the four cases with $\hat{C}_3 = 0, 2, 4, 6$ for the layered topography. The graphical correlation for the case with $\hat{C}_3 = 0$ clearly converges to the value -1 while the graphical correlation for the other cases with non-zero third invariant clearly level off for the largest values of τ and clearly do not asymptote to -1; increasing values of $\hat{C}_3$ lead to increasing values of the graphical correlation. Fig. 2 provides quantitative evidence that the coarse-grained large scale mean flows do not satisfy the predictions of the energy-enstrophy statistical theory, unless the invariant $\hat{C}_3$ vanishes identically. To confirm this, in Fig. 3 we present scatter plots of the large scale mean stream function $\langle\psi\rangle_\tau$ and mean potential vorticity, $\langle q\rangle_\tau$, for the largest averaging window, $\tau = 10^4$ from Fig. 2 for the four cases with varying $\hat{C}_3$. For the case with $\hat{C}_3 = 0$ in Fig. 3, the scatter plot shows collinear behavior while the scatter plots for the cases with increasing skewness display

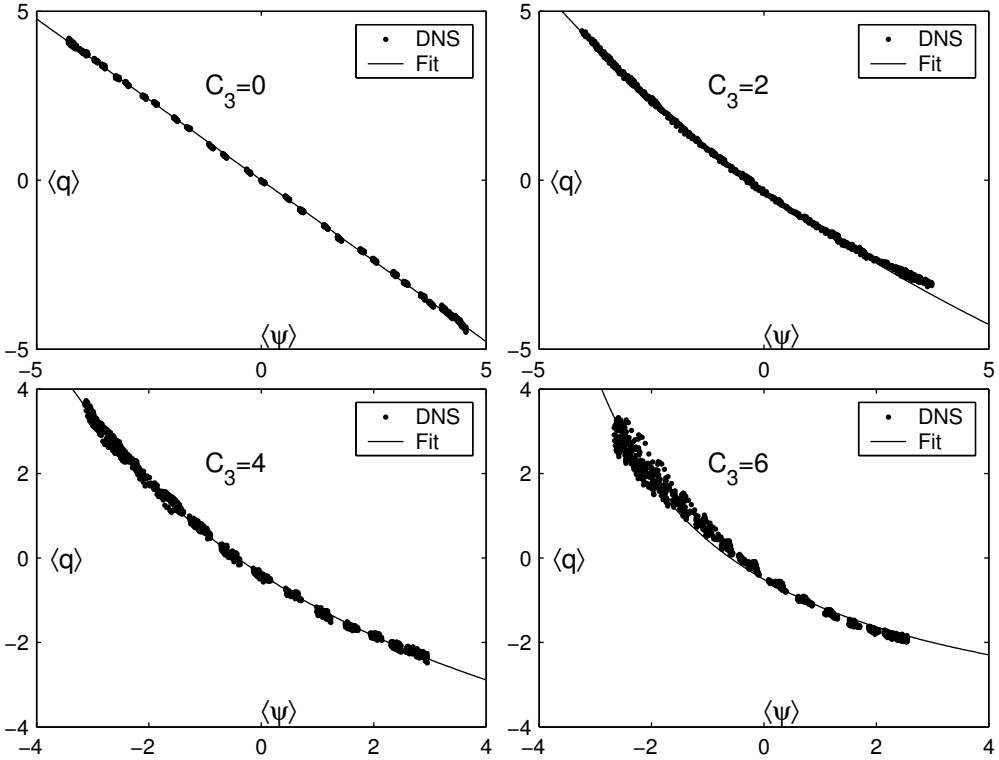

Fig. 3. The scatterplots $\bar{q}$ vs $\bar{\psi}$ for the 23×23 sine-bracket truncation, layered topography, $\hat{C}_3 = 0,\ 2,\ 4,\ 6$.

a coherent nonlinear relationship between $\bar{\psi}$ and $\bar{q}$ with increasing curvature as $\hat{C}_3$ increases through the values $2,\ 4,\ 6$. Fig. 3 provides powerful evidence for the nontrivial effect of the third invariant, $\hat{C}_3$, on the large scale coarse-grained statistical mean flow. This nontrivial effect of $\hat{C}_3$ is clearly evident in the contour plots for the coarse grained stream functions depicted in Fig. 4, plotted in each case over one period interval in x and y. For $\hat{C}_3 = 0$ the stream function is clearly layered in y as predicted by the energy-enstrophy statistical theory. This information from Fig. 4 combined with that in Fig. 2 and Fig. 3 for the case with $\hat{C}_3 = 0$ indicates that as regards the coarse grained mean flow, the energy-enstrophy statistical theory predicts the behavior; thus, with $\hat{C}_3 = 0$, the other nineteen conserved quantities, $\hat{C}_N$, $4 \leq N \leq 22$ in **10** are statistically irrelevant for predicting the large scale mean flow. On the other hand, the streamline contours in Fig. 4 b),c),d) indicate stronger more localized regions of closed stream lines associated with negative values of the stream function for the cases with $\hat{C}_3 = 2, 4, 6$. Recall that closed stream lines with negative stream function (pressure) correspond to positive (cyclonic) relative vorticity. Thus, the stream line contours in Fig. 4 indicate the presence of coherent structures through positive cyclonic vortices for positive values of the regularized third moment $\hat{C}_3$; for the case with $\hat{C}_3 = 2$, there are both cyclonic and anti-cyclonic vortices while for the cases with $\hat{C}_3 = 4, 6$, there are only cyclonic vortices in the mean stream function with increasingly weaker anti-cyclonic flow without coherent vortices. This is further strong evidence demonstrating the statistical relevance of $\hat{C}_3$ in determining the coarse grained large scale mean flow.

The Energy Spectrum

Recall that the energy-enstrophy theory predicts the equipartition of the pseudo-energy variables $\hat{p}_{\mathbf{k}}$ defined in **8** for perturbations of the mean flow in **7**. In Fig. 5 the energy spectrum of the pseudo-energy variables $\hat{p}_{\mathbf{k}}$ from **8** is plotted for perturbations of the mean flow calculated from the numerical output as in Fig. 2, Fig. 3, and Fig. 4 above for the three cases with no topography, random topography, and layered topography with $\hat{C}_3$ varying for $0,\ 4,\ 6$. It is remarkable that this energy spectrum is virtually identical for the three different large scale topographies and fixed values of $\hat{C}_3$ with $E = 7$ and $\mathcal{E} = 20$; this indicates a potentially universal feature of the spectrum for fluctuations which depends on $\hat{C}_3$ but is independent of the large scale mean flow. In particular, for the case in Fig. 5 with $\hat{C}_3 = 0$, equipartition of pseudo-energy is confirmed as predicted by the energy-enstrophy statistical theory; this is a further numerical confirmation of the statistical irrelevance of the nineteen higher order invariants $\hat{C}_N$, $4 \leq N \leq 22$, for the energy spectrum. The cases with $\hat{C}_3 = 4, 6$ in Fig. 5 clearly demonstrate the statistical relevance of this invariant in determining the energy spectrum with more pseudo-energy concentrated at small wave numbers and lower pseudo-energy at large wave numbers in a statistically identical fashion for the three cases with varying topography.

The Probability Distribution Function of Potential Vorticity

While the mean stream function emphasizes the role of $\hat{C}_3$ in determining the coarse grained large scale flow, the probability distribution function (PDF) for potential vorticity highlights the effect of $\hat{C}_3$ on the small scale fluctuations. Here this PDF is determined by a standard bin counting algorithm (27) as time evolves with evaluation at a grid of spatial points. The PDF of potential vorticity is depicted in Fig. 6 for the case with layered topography and $\hat{C}_3 = 0, 2, 4, 6$. The variance and skewness of this PDF for varying $\hat{C}_3$ are recorded in Tab. 1. The main trends apparent from Fig. 6 and Tab. 1 is the nontrivial increase in the

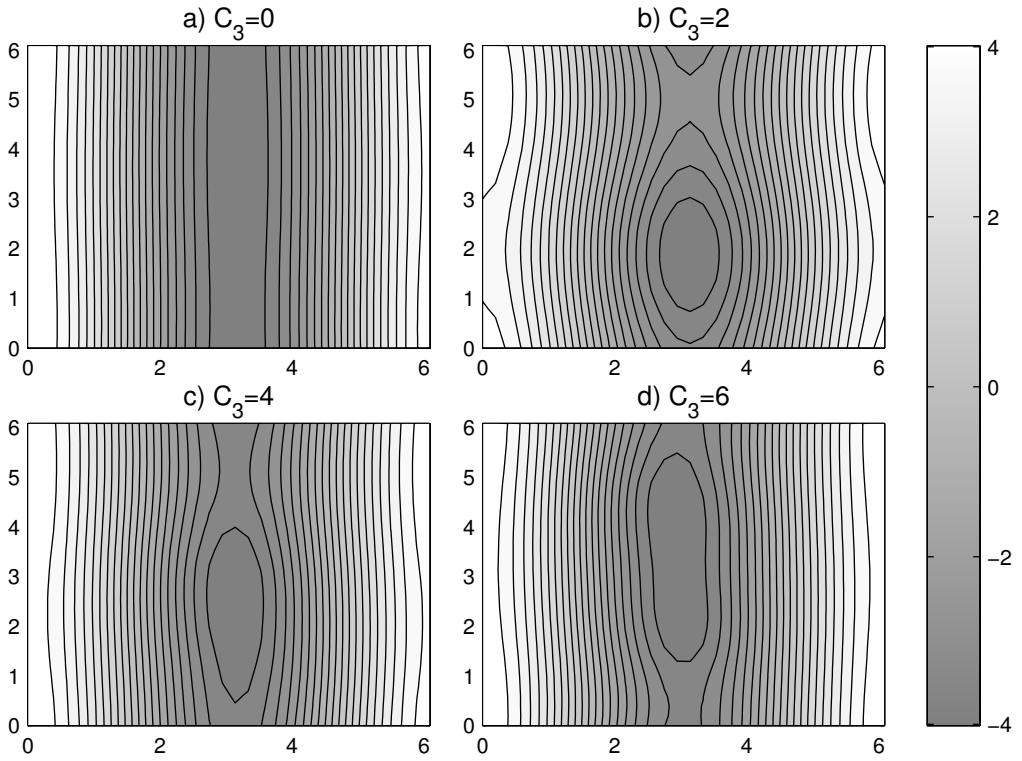

Fig. 4. The contour plots of the mean stream function, 23×23 sine-bracket truncation, layered topography, $\hat{C}_3 = 0,\ 2,\ 4,\ 6$.

positive skewness of the PDF for potential vorticity as $\hat{C}_3$ increases coupled with the nearly Gaussian PDF for potential vorticity for $\hat{C}_3 = 0$ which is predicted from the energy-enstrophy statistical theory. Once again this last result suggests the statistical irrelevance of the invariants $\hat{C}_N$, $4 \le N \le 22$ in the regime with $\hat{C}_3 = 0$ for $E = 7$, $\mathcal{E} = 20$.

$\hat{C}_3$	Variance	Skewness
0	65.67	$-1.37 \cdot 10^{-2}$
2	56.14	0.3114
4	50.82	0.7752
6	48.08	1.441

Tab. 1. Variance and skewness of PDF of the potential vorticity, $\hat{C}_3 = 0,\ 2,\ 4,\ 6$

Equilibrium Statistical Predictions of the Nonlinear Mean State

The graphs in Fig. 3 and Fig. 6 indicate that increasing the third invariant $\hat{C}_3$ systematically results in simultaneously an increasing skewness in the PDF for potential vorticity which represents small scale fluctuations and increasing nonlinearity in the scatter plot of mean stream function versus mean potential vorticity reflecting large scale behavior. A recently developed equilibrium statistical theory (2, 3, 7, 13, 19) begins with the PDF for the potential vorticity reflecting small scale fluctuations as a prior distribution and predicts the equilibrium coarse grained large scale mean flow in the continuum limit through a specific large scale functional relation, $\bar{q} = G(\bar{\psi})$. Here the nonlinear function G depends on the large scale energy and circulation constraints in a specific fashion (2, 3, 7, 13, 19). In particular, in (7) it is shown that a skewed prior distribution for small scale potential vorticity fluctuations given by the centered Gamma distribution with mean zero, variance σ, and skewness ε yields the equilibrium statistical prediction for the large scale mean flow,

$$\bar{q} = \frac{\sigma(\theta\bar{\psi} - \gamma)}{4\pi^2 - \varepsilon\sigma^{1/2}(\theta\bar{\psi} - \gamma)}. \qquad \textbf{[13]}$$

In **13**, θ and γ are Lagrange multipliers to satisfy the energy and zero circulation constraints. This modeling strategy successfully predicts the large scale coherent spots on Jupiter from the small scale Gamma prior distribution motivated by recent observations from the Galileo mission (7). Here we address the much more limited issue: if one approximates the skewed PDFs for potential vorticity in Fig. 6 by the centered Gamma distributions with the same skewness and flatness in Tab. 1 as $\hat{C}_3$ varies, are there values of the Lagrange multipliers θ, γ, so that the nonlinear large scale $\bar{q} \leftrightarrow \bar{\psi}$ relation in **13** fits the data in Fig. 3? The answer is yes and the results are the curved lines overlayed on Fig. 3. While these results are encouraging, the reader is warned that they are not a confirmation of the equilibrium statistical theory directly: if θ and γ are utilized as Lagrange multipliers to match the energy, $E = 7$, and zero circulation, the vorticity-stream relations show significantly less curvature and the stream functions are significantly nonlinear but without closed stream lines as depicted in Fig. 4. This is not surprising since simulations with 23×23 Fourier modes are extremely far from the continuum limit which requires strict spatial scale separation between the large scale flow and the small scale potential vorticity fluctuations (19, 28). Nevertheless, such trends are already evident in Fig. 3, Fig. 6, Tab. 1, and **13**.

Summary Discussion

Through unambiguous numerical experiments with the discrete approximation in **9** with many conserved quantities, it has been demonstrated that the third nonlinear invariant, $\hat{C}_3$, is statistically relevant at large scales for truncated quasi-geostrophic flow with topography. The statistical relevance

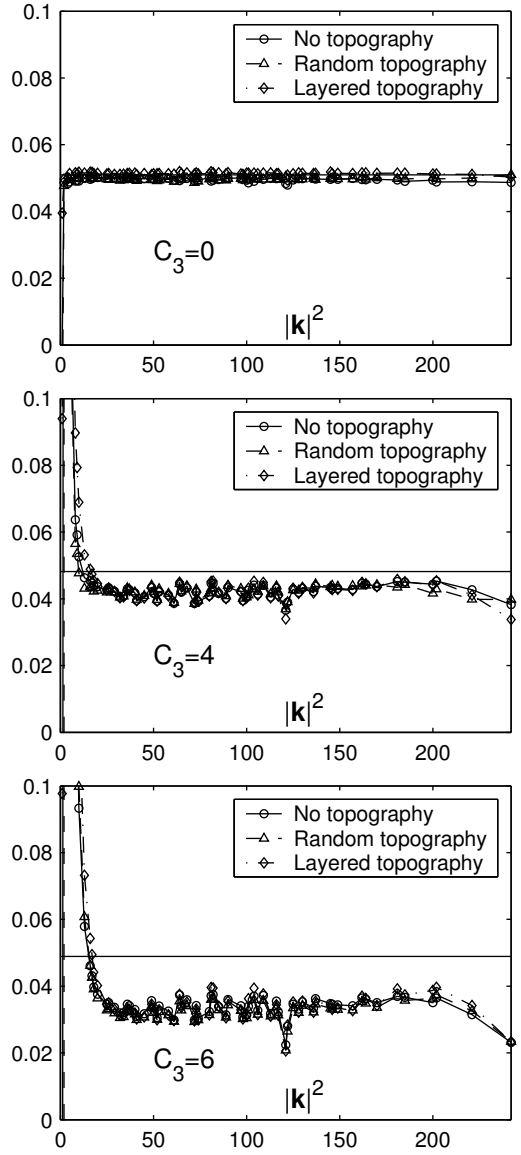

Fig. 5. The pseudo-energy spectrum, 23×23 sine-bracket truncation, different topographies, $\hat{C}_3 = 0,\ 4,\ 6$. The pseudo-energy spectrum does not depend on topography.

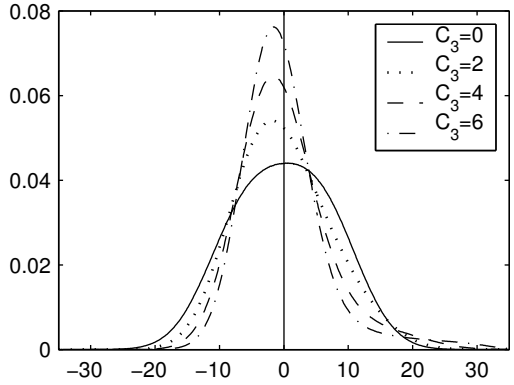

Fig. 6. The PDFs of the potential vorticity for $\hat{C}_3 = 0,\ 2,\ 4,\ 6$. Note the increasing skewness in PDFs as $\hat{C}_3$ increases.

of $\hat{C}_3$ has been demonstrated for the mean stream function and mean potential vorticity, the pseudo-energy spectrum, and the PDF for potential vorticity in a self-consistent fashion. For example, systematic increases in $\hat{C}_3$ lead to a systematic increase in nonlinearity for the mean flow with large scale coherent positive vortices as well as a systematic increase in the positive skewness of the PDF for potential vorticity. In contrast, numerical simulations not depicted here (see (21)) with the traditional spectral truncation in **6** with only the energy and enstrophy as conserved quantities reproduce the equilibrium statistical predictions in **7**, **8** for any of the initial values of $\hat{C}_3$. Also, the simulations with **9** reported above strongly suggest that the other nineteen conserved quantities, $\hat{C}_N$, $4 \leq N \leq 22$, are statistically irrelevant when $\hat{C}_3 = 0$ in the regime studied here. The issues of statistically relevant conserved quantities have been studied recently by the authors in a much more complete fashion for a simpler model involving suitable Galerkin truncations of the Burgers-Hopf equations (20, 24, 25, 27) including comparison and prediction with equilibrium microcanonical Monte-Carlo simulations. The authors hope that the present contribution as well as this recent work inspires other theoreticians to address the fundamental issues of statistically relevant conserved quantities for geophysical flows.

The research of Andrew Majda is partially supported by National Science Foundation Grant DMS-9972865 and Office of Naval Research Grant N00014-96-1-0043. Rafail Abramov is supported as a postdoctoral fellow through these grants.

1. Holloway, G. (1992) *J. Phys. Oceanogr.* **22**, 1033–1046.
2. DiBattista, M. & Majda, A. (2000) *J. Phys. Oceanogr.* **30**, 1325–1353.
3. DiBattista, M., Majda, A., & Marshall, J. (2002) *J. Phys. Oceanogr.* **32**, 599–626.
4. Kazantsev, E., Sommeria, J., & Verron, J. (1998) *J. Phys. Oceanogr.* **28**, 1017–1042.
5. Schubert, W., Montgomery, M., Taft, R., Guinn, T., Fulton, S., Kossin, J., & Edwards, J. (1999) *J. Atmos. Sci.* **56**, 1197–1223.
6. Frederiksen, J., Dix, M., & Kepert, S. (1996) *J. Atmos. Sci.* **53**, 887–904.
7. Turkington, B., Majda, A., Haven, K., & DiBattista, M. (2001) *Proc. Natl. Acad. Sci.* **98**, 12346–12350.
8. Kraichnan, R. (1975) *J. Fluid Mech.* **67**, 155–175.
9. Kraichnan, R. & Montgomery, D. (1980) *Rep. Prog. Phys.* **43**, 548–619.
10. Salmon, R., Holloway, G., & Hendershott, M. (1976) *J. Fluid Mech.* **75**, 691–703.
11. Carnevale, G. & Frederiksen, J. (1987) *J. Fluid Mech.* **175**, 153–181.
12. Salmon, R. (1998) *Lectures on Geophysical Fluid Dynamics* (Oxford Press, New York).
13. Majda, A. & Wang, X. (2003) *Nonlinear Dynamics and Statistical Theories for Basic Geophysical Flow* (Cambridge Univ. Press, New York), in press.
14. Holloway, G. (1986) *Annu. Rev. Fluid Mech.* **18**, 49–65.
15. Merryfield, W. & Holloway, G. (1996) *J. Fluid Mech.* **309**, 85–91.
16. Miller, J., Weichman, P., & Cross, M. (1992) *Phys. Rev.* **A45**, 2328–2359.
17. Onsager, L. (1949) *Nuovo Cimento* **6**, 279–287.
18. Montgomery, D. & Joyce, G. (1974) *Phys. Fluids* **17**, 1139–1147.
19. Turkington, B. (1999) *Comm. Pure Appl. Math.* **52**, 781–809.
20. Abramov, R. & Majda, A. (2003) Discrete approximations with additional conserved quantities: Deterministic and statistical behavior, accepted 11/20/02 to J. Math. Anal. App. and in press.
21. Abramov, R. (2002), PhD thesis, Rensselaer Polytechnic Institute, Supervised by A. Majda and G. Kovačič.
22. Zeitlin, V. (1991) *Physica D* **49**, 353–362.
23. McLachlan, R. (1993) *Phys. Rev. Lett.* **71**, 3043–3046.
24. Majda, A. & Timofeyev, I. (2000) *Proc. Natl. Acad. Sci.* **97**(23), 12413–12417.
25. Majda, A. & Timofeyev, I. (2002) *Milan Journal of Mathematics* **70**, 39–96.
26. Kells, L. & Orszag, S. (1978) *Phys. Fluids* **21**, 162–168.
27. Abramov, R., Kovačič, G., & Majda, A. (2003) *Comm. Pure Appl. Math.* **56**, 0001–0046.
28. Ellis, R., Haven, K., & Turkington, B. (2003) Analysis of statistical equilibrium models of geostrophic turbulence, accepted to J. Appl. Math. Stoch. Anal.